ChemComm

Ethyl Methyl Sulfone Co-Solvent Eliminates Macroscopic Morphological Instabilities of Lithium Metal Anode

Journal:	*ChemComm*
Manuscript ID	CC-COM-01-2019-000046.R1
Article Type:	Communication

Journal Name

COMMUNICATION

Ethyl Methyl Sulfone Co-Solvent Eliminates Macroscopic Morphological Instabilities of Lithium Metal Anode

Woochul Shin,[a] Kang Pyo So,[b] William F. Stickle,[c] Cong Su,[b] Jun Lu,[d] Ju Li,[b,*] and Xiulei Ji [a,*]

Received 00th January 20xx,
Accepted 00th January 20xx

DOI: 10.1039/x0xx00000x

www.rsc.org/

Lithium metal anode suffers a short cycle life, and the parasitic reactions of lithium with the electrolytes are widely observed. The common sense is to avoid such reactions. Herein, we head to the opposite direction by using an oxidizing co-solvent of ethyl methyl sulfone in the electrolyte, which addresses the 'dendrite' issue entirely, resulting in dense and macroscopically smooth surface morphology of the plated lithium. However, the dendrite-free lithium metal anode does not necessarily exhibit a high Coulombic efficiency.

Lithium metal anode (LMA) is supposed to be the ultimate solution to facilitate the long-driving range of electric vehicles (EV). The challenges of LMA are twofold: (1) lithium morphological instabilities (LMI) during plating/stripping that may cause shorting and thermal runaway and (2) the low Coulombic efficiency (CE). LMI can be categorized into 'dendrite or tip grown' (mode III), stress-derived 'whisker or root grown' (mode II), and the combination of the two (mode I).[1] To prevent LMI, various strategies have been developed such as 3D electrode architectures,[2–5] electrolyte additives, e.g., Cs salts,[6] and new SEI design.[7] Recently, high concentrations of electrolyte salts, particularly with the fluorinated ones, have been demonstrated capable of improving both (1) and (2) on LMA.[8,9] To avoid LMI, a common-sense route might be to mitigate the parasitic reactions between the electrolytes and LMA. This favours the usage of cathodically more stable electrolytes, such as ionic liquids.[10–13]

Herein, we report that ethyl methyl sulfone (EMS) as a co-solvent to the ether-based electrolyte eliminates macroscopically observable LMI. Sulfone-containing electrolytes, including EMS, are known for their remarkable anodic stability but high cathodic reactivity.[14–17] Recently, high concentrations of salts solvated by sulfolane (TMS) have been studied on LMA as promising electrolytes.[18,19] In this work, we reveal that LMA exhibits dendrite-free plating/stripping behaviour in an electrolyte of 1 M bis(trifluoromethanesulfonyl)imide (LiTFSI) solvated in 50 v% of EMS, 25 v% 1,3-dioxolane (DOL), and 25 v% 1,2-dimethoxyethane (DME) (referred to as EMS/DOL/DME). However, in the Li || Cu asymmetric cells, LMA demonstrates a CE of only 30% in the above electrolyte. Surprisingly, the cure of macroscopic LMI does not necessarily lead to high CE.

We first employed Li || Li symmetric coin cells to reveal the impacts of adding EMS as a co-solvent in the electrolyte. Scanning electron microscopy (SEM) imaging shows the surface morphology of LMA after 100 galvanostatic plating/stripping cycles at 1.0 mA cm^{-2} with a capacity of 1.0 mAh cm^{-2} in two electrolytes of 1 M LiTFSI in DOL/DME (50 v% / 50 v%) (referred to as DOL/DME) and EMS/DOL/DME. In DOL/DME, LMA exhibits completely pulverized surface covered by lithium particles (Fig. 1a). In contrast, the EMS/DOL/DME electrolyte leads to exceptionally flat and smooth surface entirely free of any LMI from face (Fig. 1b,c). This smooth configuration can be observed across the entire lithium metal surface, as shown in multiple-scale ranges (Fig. S1, ESI†) Similarly, the side view of LMA reveals the formation of the mode-III LMI (Fig. 1d) in DOL/DME compared to no LMI formation in EMS/DOL/DME (Fig. 1e) with optical observations. The corresponding energy dispersive X-ray spectroscopy (EDX) elemental mappings reveal that the LMA's surface in the EMS/DOL/DME electrolyte is uniformly covered by sulphur- and fluorine-containing species, which constitute the SEI (Fig. S2, ESI†).

In situ optical microscopy imaging was performed in vial cells to monitor the morphological change during the plating process at a current density of 0.3 mA cm^{-2} for 4 hours with a capacity of 1.2 mAh cm^{-2} in two different electrolytes (Fig. S3, ESI†). Fig. 1e shows that

[a] *Department of Chemistry, Oregon State University, Corvallis, OR, 97331, United States. Email: david.ji@oregonstate.edu*
[b] *Department of Nuclear Science and Engineering and Department of Materials Science and Engineering, Massachusetts Institute of Technology, Cambridge, MA, 02139, United States. Email: liju@mit.edu*
[c] *Hewlett-Packard Co., 1000 NE Circle Blvd., Corvallis, OR, 97330, United States.*
[d] *Chemical Sciences and Engineering Division, Argonne National Laboratory, Argonne, IL, 60439, United States*
† *Electronic Supplementary Information (ESI) available: Experimental details, EDX, in situ* microscopy, and F_{1s} XPS. *See DOI: 10.1039/x0xx00000x*

mossy-like LMI are formed during plating in the DOL/DME electrolyte (red arrows), and these are not fully removed in the following stripping process (red circles).[20] During the 2nd plating, LMI are formed on the fresh lithium spots, where we expect that continuous 'dead' lithium formation will eventually cover the lithium upon cycling, consequently leading to lower CE. On the other hand, the EMS/DOL/DME electrolyte shows no obvious LMI formation and maintains the original surface morphology of LMA. However, during the first plating, bubbles are formed, which was not observed in DOL/DME. The bubble formation may release some of the carbon-containing moieties of the EMS, thus leaving a SEI on the surface of LMA containing less organic but more inorganic constituents.

The galvanostatic plating/stripping tests using Li || Li symmetric cells at 2 mA cm^{-2} with a capacity of 3 mAh cm^{-2} reveals the performance juxtaposition of the two electrolytes. The DOL/DME electrolyte exhibits high overpotentials: from 50 to 110 cycles ranging from 150 to 400 mV and just below 100 mV afterwards (Fig. 2a and the inset), whereas the EMS/DOL/DME electrolyte exhibits consistently low overpotential of 15 mV.

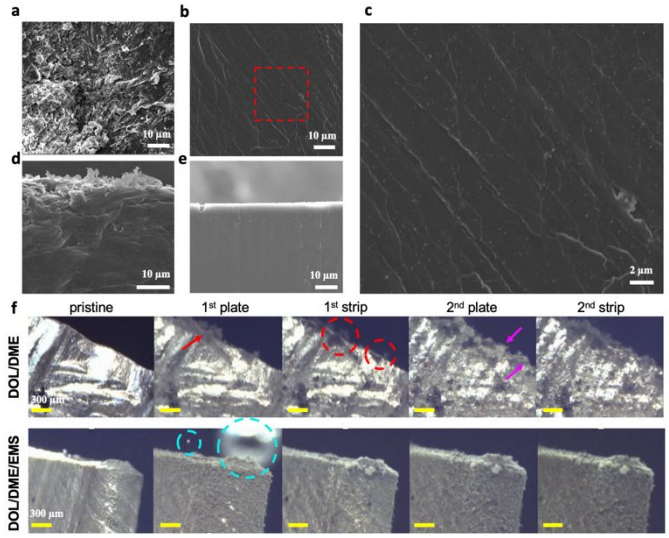

Figure 1. Morphology studies of the cycled lithium surface. (a-e) SEM images of LMA examined after 100 cycles at 1.0 mA cm^{-2} with a capacity of 1.0 mAh cm^{-2}. LMA urface in (a) DOL/DME, (b) EMS/DOL/DME, (c) An enlarged image of the red box in (b). Cross section in (d) DOL/DME, (e) EMS/DOL/DME. (f) *In situ* optical images of LMA in DOL/DME (top) and EMS/DOL/DME (bottom) electrolytes. Current density is 0.3 mA cm^{-2} with a capacity of 1.2 mAh cm^{-2}. Arrows and circles in DOL/DME indicate LMI on LMA. Circles in the second image (bright blue) for EMS/DOL/DME denotes the gas bubbles. The scale bar for all images is 300 μm.

Cyclic voltammetry (CV) tests of Li || Cu asymmetric cells where a Cu current collector serves as the working electrode reveal the very different behaviours of LMA in electrolytes with or without EMS. In DOL/DME, the cathodic current and anodic current progressively increase during the initial three cycles (Fig. 3b), which indicates that LMA possesses a surface area anew and larger after each cycle. However, in the EMS/DOL/DME electrolyte, the redox current remains stable during cycling, suggestive the markedly more stable surface of LMA, probably due to the favourable SEI formation (Fig. 3c). However, in the galvanostatic plating/stripping tests, the LMA exhibits a surprisingly low first-cycle CE of 30% (Fig. S4 ESI†), which indicates that the overwhelming majority of the plated lithium is consumed, i.e., for building the SEI layer, which stems from the fact that EMS's reactivity toward lithium is very high.

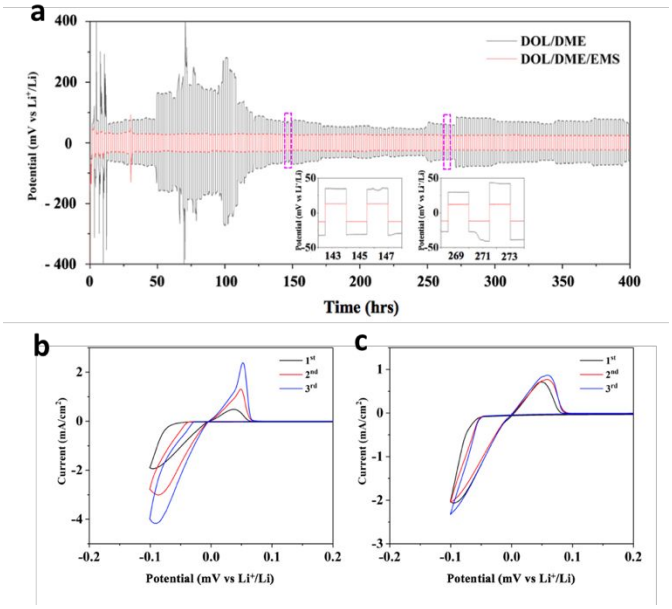

Figure 2. (a) Electrochemical studies in Li | | Li symmetric cells. Potential profiles of Li symmetric cells with the DOL/DME electrolyte and the EMS/DOL/DME electrolyte at the current density of 2.0 mA cm^{-2} with a capacity of 3.0 mA h cm^{-2}. Insets represent the 48th cycle (left) and the 90th cycle (right), respectively. CV profiles of the first three cycles in (b) DOL/DME (c) EMS/DOL/DME.

Recently, the SEI layers on LMA are described by a dual-layer model with an organic layer on top of an inorganic layer. To understand the SEI structures of LMA in EMS/DOL/DME, we collected *ex situ* XPS spectra on the LMA surface after 100 stripping/plating cycles with depth-profiling by Ar^+ sputtering. The entire sputtering process lasts for four minutes, where one spectrum was collected after every minute of sputtering. The results reveal that the LMA in EMS/DOL/DME comprises a thinner organic layer than LMA does in DOL/DME. The characteristic species of the organic layer of SEI, including Li_2CO_3, $(CH_3CH_2OCH_2O\text{-})_n$, $(CH_3CH_2O\text{-R})_n$, and C-C peaks all disappear after two minutes of sputtering on LMA from EMS/DOL/DME, whereas all these peaks still remain on the LMA from DOL/DME even after four minutes' sputtering (Fig. 3a). A meagre organic layer of SEI on LMA in EMS/DOL/DME suggests that an inorganic layer of SEI formed with the assistance of EMS blocks the diffusion of DOL/DME solvent molecules.

We further studied the composition of the inorganic layer of SEI by sulphur and oxygen depth profiles (Fig. 3b and c). For both electrolytes, the $–SO_2$/$–SO_3$ peaks diminish along the depth,

and both Li_2S_x ($1 \leq x \leq 2$) and Li_2O peaks emerge and grow upon further sputtering. Furthermore, the EMS/DOL/DME electrolyte shows a more rapid attenuation of the peaks for $–SO_2$/$–SO_3$ when going deeper during profiling. Compared to DOL/DME, EMS/DOL/DME exhibits weaker peak intensity of Li_2S and a more prominent presence of Li_2O. In addition, it is evident that EMS is preferentially decomposed over LiTFSI due to the fact that the fluorine signal only comes from $TFSI^-$ anion, and the LMA in EMS/DOL/DME displays a weaker F_{1s} peak throughout the depth of SEI than DOL/DME (Fig. S5 ESI†).

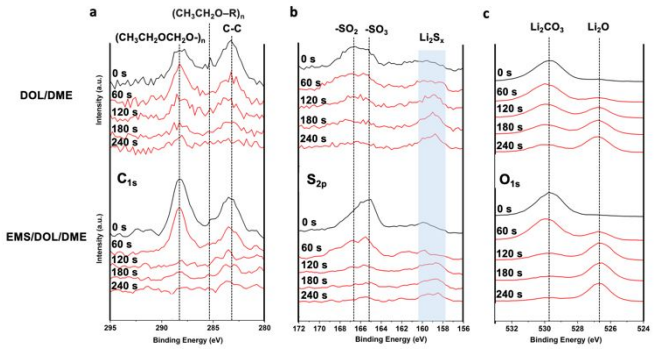

Figure 3. The XPS profiles of the cycled LMA in DOL/DME electrolyte (top) and EMS/DOL/DME electrolyte (bottom) for (a) C_{1s}, (b) S_{2p} and (c) O_{1s}. Sputtering was carried out for 4 minutes with one scanning in every minute.

In summary, our results demonstrate that EMS completely suppresses macroscopic LMI on LMA, and facilitates extremely smooth surface morphology of LMA. The profiling XPS results reveal that EMS preferentially decomposes over DOL/DME and LiTFSI on the surface of LMA, generating a thinner organic layer near the electrode. Although EMS/DOL/DME does not seem to be practically apt as the electrolyte for LMA, its function to cause complete dendrite-free lithium plating warrants future attention on EMS as an electrolyte additive. We tentatively posit that the reaction between EMS and LMA may dramatically increase the total concentration of ions (ionic strength) near LMA, which prevents the formation of a Sand's extinction zone in the liquid where the ionic strength approaches zero.[21,22]

Conflicts of interest

There are no conflicts to declare.

Notes and references

1 S. Li, M. Jiang, Y. Xie, H. Xu, J. Jia and J. Li, *Advanced Materials*, 2018, **30**, 1706375.
2 Z. Liang, D. Lin, J. Zhao, Z. Lu, Y. Liu, C. Liu, Y. Lu, H. Wang, K. Yan, X. Tao and Y. Cui, *PNAS*, 2016, **113**, 2862–2867.
3 Y. Zhang, W. Luo, C. Wang, Y. Li, C. Chen, J. Song, J. Dai, E. M. Hitz, S. Xu, C. Yang, Y. Wang and L. Hu, *PNAS*, 2017, **114**, 3584–3589.
4 G. Zheng, S. W. Lee, Z. Liang, H.-W. Lee, K. Yan, H. Yao, H. Wang, W. Li, S. Chu and Y. Cui, *Nat Nano*, 2014, **9**, 618–623.
5 X. Ji, D.-Y. Liu, D. G. Prendiville, Y. Zhang, X. Liu and G. D. Stucky, *Nano Today*, 2012, **7**, 10–20.
6 F. Ding, W. Xu, G. L. Graff, J. Zhang, M. L. Sushko, X. Chen, Y. Shao, M. H. Engelhard, Z. Nie, J. Xiao, X. Liu, P. V. Sushko, J. Liu and J.-G. Zhang, *J. Am. Chem. Soc.*, 2013, **135**, 4450–4456.
7 X.-B. Cheng, C. Yan, X. Chen, C. Guan, J.-Q. Huang, H.-J. Peng, R. Zhang, S.-T. Yang and Q. Zhang, *Chem*, 2017, **2**, 258–270.
8 L. Suo, W. Xue, M. Gobet, S. G. Greenbaum, C. Wang, Y. Chen, W. Yang, Y. Li and J. Li, *PNAS*, 2018, 201712895.
9 H.-G. Jung, J. Hassoun, J.-B. Park, Y.-K. Sun and B. Scrosati, *Nature Chemistry*, 2012, **4**, 579–585.
10 D. Aurbach, A. Zaban, A. Schechter, Y. Ein-Eli, E. Zinigrad and B. Markovsky, *J. Electrochem. Soc.*, 1995, **142**, 2873–2882.
11 C. Zu, N. Azimi, Z. Zhang and A. Manthiram, *Journal of Materials Chemistry A*, 2015, **3**, 14864–14870.
12 A. I. Bhatt, A. S. Best, J. Huang and A. F. Hollenkamp, *J. Electrochem. Soc.*, 2010, **157**, A66–A74.
13 G. H. Lane, P. M. Bayley, B. R. Clare, A. S. Best, D. R. MacFarlane, M. Forsyth and A. F. Hollenkamp, *J. Phys. Chem. C*, 2010, **114**, 21775–21785.
14 A. Abouimrane, I. Belharouak and K. Amine, *Electrochemistry Communications*, 2009, **11**, 1073–1076.
15 K. Xu and C. A. Angell, *J. Electrochem. Soc.*, 2002, **149**, A920–A926.
16 N. Shao, X.-G. Sun, S. Dai and D. Jiang, *J. Phys. Chem. B*, 2011, **115**, 12120–12125.
17 United States, US6245465B1, 2001.
18 J. Alvarado, M. A. Schroeder, M. Zhang, O. Borodin, E. Gobrogge, M. Olguin, M. S. Ding, M. Gobet, S. Greenbaum, Y. S. Meng and K. Xu, *Materials Today*, 2018, **21**, 341–353.
19 X. Ren, S. Chen, H. Lee, D. Mei, M. H. Engelhard, S. D. Burton, W. Zhao, J. Zheng, Q. Li, M. S. Ding, M. Schroeder, J. Alvarado, K. Xu, Y. S. Meng, J. Liu, J.-G. Zhang and W. Xu, *Chem*, 2018, **4**, 1877–1892.
20 A. Kushima, K. P. So, C. Su, P. Bai, N. Kuriyama, T. Maebashi, Y. Fujiwara, M. Z. Bazant and J. Li, *Nano Energy*, 2017, **32**, 271–279.
21 M. D. Tikekar, S. Choudhury, Z. Tu and L. A. Archer, *Nature Energy*, 2016, **1**, 16114.
22 H. J. S. S. Ph.D, *The London, Edinburgh, and Dublin Philosophical Magazine and Journal of Science*, 1901, **1**, 45–79.

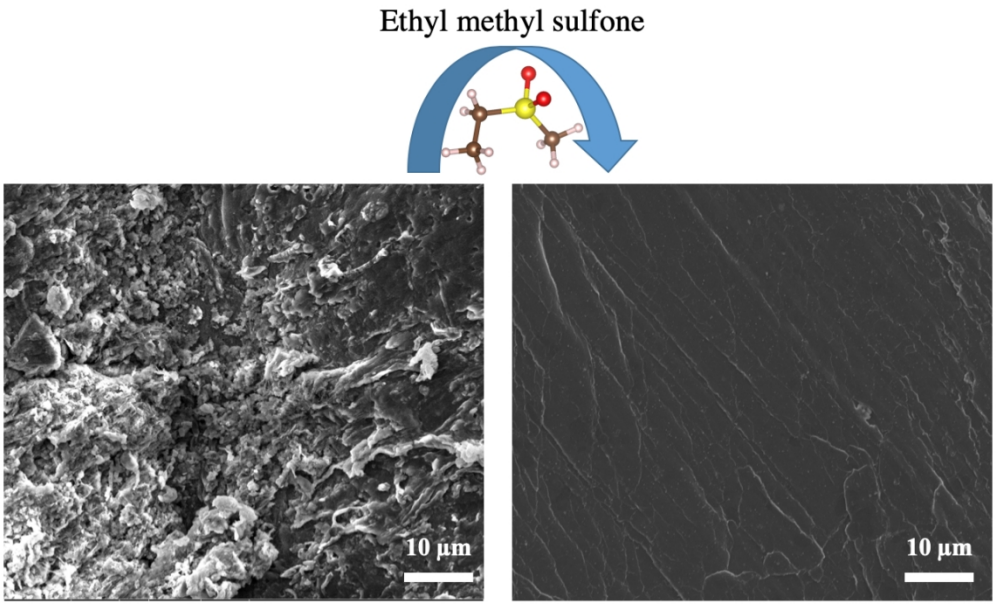
Ethyl methyl sulfone
10 µm
10 µm